Journal of Guidance, Control, and Dynamics
Vol. 35, No. 2, March–April 2012

Engineering Notes

Symplectic Approaches for Solving Two-Point Boundary-Value Problems

Haijun Peng,* Qiang Gao,† Zhigang Wu,‡ and Wanxie Zhong§
Dalian University of Technology, 116024 Dalian, People's Republic of China

DOI: 10.2514/1.55795

I. Introduction

THE two-point boundary-value problem (TPBVP) plays a fundamental role in optimal control problems of aerospace engineering, including the problem of spacecraft orbit transfer [1], the optimal reconfiguration of spacecraft formations [2], and continuous thrust rendezvous problems [3]. Therefore, many techniques and methods for solving TPBVP have been proposed and developed [4–7].

The optimal control problem is as follows. The dynamic system is

$$\dot{\mathbf{x}}(t) = f(\mathbf{x}(t), \mathbf{u}(t), t) \tag{1}$$

and the goal is to minimize the following cost function:

$$J = h(\mathbf{x}(t_f), t_f) + \int_0^{t_f} \Phi(\mathbf{x}(t), \mathbf{u}(t), t)\, \mathrm{d}t \tag{2}$$

in which t denotes time, the dot represents the derivative with respect to time, $\mathbf{x}$ is a d-dimensional state vector, $\mathbf{u}$ is a p-dimensional control input vector, and J is a cost function. In this Note, we mainly focus on the optimal control problem with a fixed terminal time, i.e., t_f is given.

Assume that the control input is unconstrained. By introducing the Lagrangian multiplier $\boldsymbol{\lambda}$ and the Hamiltonian function

$$\bar{H}(\mathbf{x}, \mathbf{u}, \boldsymbol{\lambda}) = \Phi(\mathbf{x}(t), \mathbf{u}(t), t) + \boldsymbol{\lambda}^T f(\mathbf{x}(t), \mathbf{u}(t), t)$$

the necessary condition for the optimal control input can be derived by the standard variational approach [8] as follows:

$$\frac{\partial \bar{H}(\mathbf{x}, \mathbf{u}, \boldsymbol{\lambda}, t)}{\partial \mathbf{u}} = 0 \tag{3}$$

Without loss of generality, assume that the control input $\mathbf{u}$ can be expressed by the state variable $\mathbf{x}$ and the costate variable $\boldsymbol{\lambda}$, i.e., $\mathbf{u}(t) = g(\mathbf{x}(t), \boldsymbol{\lambda}(t))$. Then, a new Hamiltonian function $H(\mathbf{x}, \boldsymbol{\lambda})$, which depends only on the state and costate variables, can be given as follows:

$$H(\mathbf{x}, \boldsymbol{\lambda}) = \Phi(\mathbf{x}(t), g(\mathbf{x}, \boldsymbol{\lambda}), t) + \boldsymbol{\lambda}^T f(\mathbf{x}(t), g(\mathbf{x}, \boldsymbol{\lambda}), t) \tag{4}$$

The action $\bar{S}$ in a time interval $(0, \eta)$ is defined [9] as the following:

$$\bar{S} = \int_0^{\eta} (\boldsymbol{\lambda}^T \dot{\mathbf{x}} - H)\, \mathrm{d}t \tag{5}$$

Because the terminal time is fixed, the variation for the action $\bar{S}$ yields the following:

$$\delta \bar{S} = \int_0^{\eta} (\delta \mathbf{x})^T \left(-\dot{\boldsymbol{\lambda}} - \frac{\partial H}{\partial \mathbf{x}} \right) \mathrm{d}t + \int_0^{\eta} (\delta \boldsymbol{\lambda})^T \left(\dot{\mathbf{x}} - \frac{\partial H}{\partial \boldsymbol{\lambda}} \right) \mathrm{d}t + \boldsymbol{\lambda}^T \delta \mathbf{x} \Big|_0^{\eta} = 0 \tag{6}$$

First, the variational principle equation (6) can be used to derive the nonlinear TPBVP according to the initial and terminal state conditions. For the optimal control problem, the initial state is given. In this Note, two different types of terminal state conditions are considered, i.e., the free terminal state conditions or the fixed terminal state conditions. If the terminal state is free, then the boundary conditions $\mathbf{x}(0) = \mathbf{x}_0$ and $\boldsymbol{\lambda}(t_f) = \partial h(\mathbf{x}(t_f), t_f)/\partial \mathbf{x}(t_f)$ can be given by the variational principle [8]. If the terminal state is fixed, then the boundary conditions $\mathbf{x}(0) = \mathbf{x}_0$ and $\mathbf{x}(t_f) = \mathbf{x}_f$ can be given by the variational principle [8]. The symbols $\mathbf{x}_0$ and $\mathbf{x}_f$ are the given states at the initial and terminal times, respectively. According to Eq. (6), the solutions of the optimal control problem should satisfy the following Hamiltonian canonical equation:

$$\dot{\mathbf{x}} = \frac{\partial H}{\partial \boldsymbol{\lambda}} = f(\mathbf{x}, g(\mathbf{x}, \boldsymbol{\lambda}), t), \qquad \dot{\boldsymbol{\lambda}} = -\frac{\partial H}{\partial \mathbf{x}} \tag{7}$$

So far, the nonlinear optimal control problem has been transferred into the nonlinear TPBVP of Hamiltonian systems with different boundary conditions.

The shooting and multiple shooting methods [4] can be employed to solve this TPBVP. For these methods, unknown initial states or costates must be guessed until the transversality conditions are satisfied. They can reach effective convergence but may cause ill-conditioning for a problem with a long time interval. A generating function method [3] is proposed to solve the TPBVP of Hamiltonian systems. The generating function method has an advantage over the conventional numerical shooting method in the sense that it does not require a guess of initial or terminal costates. However, complicated series expansions are needed for the generating function method.

The most fundamental property of Hamiltonian systems is that the phase flow is a symplectic transformation [9]. Numerical methods preserving the symplectic structure are more effective for solving Hamiltonian systems. For example, the symplectic method exhibits excellent energy behavior and accurately reflects the qualitative behavior of the solution [10]. Therefore, many symplectic numerical methods have been proposed and applied in solving initial-value problem of Hamiltonian systems.

The experiences for initial-value problem show that symplectic-preserving is important for designing numerical methods of Hamiltonian systems. Reference [11] proposed a symplectic method called discrete mechanics and optimal control (DMOC) for the solving optimal control problem, which shows that the application of the symplectic method to the optimal control problem has similar advantages as the initial-value problem. For example, the symplectic numerical method can preserve the energy better than the non-symplectic method, and it leads to a reasonable approximation to the continuous solution for a small number of discretization points [11,12].

From a mathematical point of view, the generating function method and the DMOC method are both symplectic. For the

Received 28 July 2011; revision received 18 September 2011; accepted for publication 23 September 2011.

*Ph.D. Candidate, Department of Engineering Mechanics; hjpeng@dlut.edu.cn.
†Lecturer, Department of Engineering Mechanics; qgao@dlut.edu.cn (Corresponding Author).
‡Professor, School of Aeronautics and Astronautics; wuzhg@dlut.edu.cn.
§Professor, Department of Engineering Mechanics; zwoffice@dlut.edu.cn.

generating function method, symbolic computation and solving of large-scale ordinary different equations may lead to significant computational efforts. For the DMOC method, the symplectic-preserving idea is only applied to discrete the dynamic equations in the optimal control system and not to the whole optimal control system. In this Note, a systematic procedure is developed to construct three symplectic approaches for solving the Hamiltonian TPBVP derived from the optimal control problem. These symplectic approaches have been used to solve an optimal rendezvous problem with fixed time and without constraints.

II. Actions Based on the Variational Principle

Since the symplectic structure plays a fundamental role in Hamiltonian systems, numerical methods that preserve the symplectic structure are desired. For a numerical approach, the continuous time domain is divided into a series of discrete time intervals, and the solutions can only be obtained on discrete time points. Therefore, assume that the relationship of a solution vector between two adjacent time points can be given by

$$\mathbf{v}_j = \boldsymbol{\Psi}(\mathbf{v}_{j-1}) \tag{8}$$

in which $\mathbf{v}_j = \{\mathbf{x}_j^T, \boldsymbol{\lambda}_j^T\}^T$ and $\boldsymbol{\Psi}$ is a mapping function in state space.

A numerical approach is symplectic if and only if the Jacobi matrix of the mapping function $\boldsymbol{\Psi}$ is a symplectic matrix [10]. The Jacobi matrix of the mapping function $\boldsymbol{\Psi}$ can be defined by

$$\mathbf{S} = \frac{\partial \mathbf{v}_j}{\partial \mathbf{v}_{j-1}} = \begin{bmatrix} \frac{\partial \mathbf{x}_j}{\partial \mathbf{x}_{j-1}} & \frac{\partial \mathbf{x}_j}{\partial \boldsymbol{\lambda}_{j-1}} \\ \frac{\partial \boldsymbol{\lambda}_j}{\partial \mathbf{x}_{j-1}} & \frac{\partial \boldsymbol{\lambda}_j}{\partial \boldsymbol{\lambda}_{j-1}} \end{bmatrix} \tag{9}$$

Therefore, if the matrix $\mathbf{S}$ satisfies the following equation,

$$\mathbf{S}^T\mathbf{J}\mathbf{S} = \mathbf{J}, \qquad \mathbf{J} = \begin{bmatrix} \mathbf{0} & \mathbf{I} \\ -\mathbf{I} & \mathbf{0} \end{bmatrix} \tag{10}$$

then the corresponding numerical approach is symplectic.

The variational principle given in Eq. (6) not only gives the Hamiltonian canonical equation but also can be used as the foundation for constructing a numerical approach. According to Eq. (6), if the Hamiltonian canonical equation is satisfied within the time interval $(0, \eta)$, then the first type of relationship between the action $\bar{S}$ and the states and costates at the two ends can be given as follows:

$$\mathrm{d}\,\bar{S} = \boldsymbol{\lambda}_\eta^T\, \mathrm{d}\mathbf{x}_\eta - \boldsymbol{\lambda}_0^T\, \mathrm{d}\mathbf{x}_0 \tag{11}$$

where $\mathbf{x}_0$ and $\boldsymbol{\lambda}_0$ are the state and costate variables at the initial time, respectively, and $\mathbf{x}_\eta$ and $\boldsymbol{\lambda}_\eta$ are the state and costate variables at time η, respectively. Equation (11) implies that if the Hamiltonian canonical equation is satisfied within the time interval, then the action $\bar{S}$ is a function of only $\mathbf{x}_0$ and $\mathbf{x}_\eta$.

The second type of relationship between the action and the state as well as the costate at two ends can also be given from Eq. (11). Because

$$\mathrm{d}\,(\boldsymbol{\lambda}_\eta^T\mathbf{x}_\eta) = \boldsymbol{\lambda}_\eta^T\, \mathrm{d}\mathbf{x}_\eta + \mathbf{x}_\eta^T\, \mathrm{d}\boldsymbol{\lambda}_\eta \tag{12}$$

Eq. (11) can be written as

$$\mathrm{d}\,(\boldsymbol{\lambda}_\eta^T\mathbf{x}_\eta) - \mathrm{d}\bar{S}(\mathbf{x}_0, \mathbf{x}_\eta) = \boldsymbol{\lambda}_0^T\, \mathrm{d}\mathbf{x}_0 + \mathbf{x}_\eta^T\, \mathrm{d}\boldsymbol{\lambda}_\eta \tag{13}$$

If we define U by

$$U = \boldsymbol{\lambda}_\eta^T\mathbf{x}_\eta - \bar{S}(\mathbf{x}_0, \mathbf{x}_\eta) \tag{14}$$

then Eq. (13) gives

$$\mathrm{d}\,U = \boldsymbol{\lambda}_0^T\, \mathrm{d}\mathbf{x}_0 + \mathbf{x}_\eta^T\, \mathrm{d}\boldsymbol{\lambda}_\eta \tag{15}$$

Equation (15) implies that, if the Hamiltonian canonical equation is satisfied within the time interval $(0, \eta)$, and the state $\mathbf{x}_0$ at the left end and the costate $\boldsymbol{\lambda}_\eta$ at the right end of the time interval are taken as the independent variables, then U must be a function of only $\mathbf{x}_0$ and $\boldsymbol{\lambda}_\eta$.

Similarly, the third type of relationship between the action and the state as well as the costate at two ends can be given as follows:

$$\mathrm{d}\,(\boldsymbol{\lambda}_0^T\mathbf{x}_0 - \boldsymbol{\lambda}_\eta^T\mathbf{x}_\eta) = \boldsymbol{\lambda}_0^T\, \mathrm{d}\mathbf{x}_0 + \mathbf{x}_0^T\, \mathrm{d}\boldsymbol{\lambda}_0 - \boldsymbol{\lambda}_\eta^T\, \mathrm{d}\mathbf{x}_\eta - \mathbf{x}_\eta^T\, \mathrm{d}\boldsymbol{\lambda}_\eta \tag{16}$$

which allows Eq. (11) to be written as

$$\mathrm{d}\,(\boldsymbol{\lambda}_0^T\mathbf{x}_0 - \boldsymbol{\lambda}_\eta^T\mathbf{x}_\eta + \bar{S}(\mathbf{x}_0, \mathbf{x}_\eta)) = \mathbf{x}_0^T\, \mathrm{d}\boldsymbol{\lambda}_0 - \mathbf{x}_\eta^T\, \mathrm{d}\boldsymbol{\lambda}_\eta \tag{17}$$

If we define V by

$$V = \boldsymbol{\lambda}_0^T\mathbf{x}_0 - \boldsymbol{\lambda}_\eta^T\mathbf{x}_\eta + \bar{S}(\mathbf{x}_0, \mathbf{x}_\eta) \tag{18}$$

then Eq. (17) gives

$$\mathrm{d}\,V = \mathbf{x}_0^T\, \mathrm{d}\boldsymbol{\lambda}_0 - \mathbf{x}_\eta^T\, \mathrm{d}\boldsymbol{\lambda}_\eta \tag{19}$$

Equation (19) implies that, if the Hamiltonian canonical equation is satisfied within the time interval $(0, \eta)$, and the costate variables $\boldsymbol{\lambda}_0$ and $\boldsymbol{\lambda}_\eta$ at two ends of the time interval are taken as the independent variables, then V must be the function of only $\boldsymbol{\lambda}_0$ and $\boldsymbol{\lambda}_\eta$.

In this section, based on the variational principle and by choosing different types of independent variables at the two ends of the time step, three different actions [Eqs. (11), (15), and (19)] are given. In the next section, three symplectic numerical approaches for solving nonlinear TPBVP are proposed based on the three different actions.

III. Symplectic Approaches Based on the Actions

For numerical integration, the time domain $(0, t_f)$ is divided into L time intervals with equal time steps $\eta = t_f/L$, i.e., $t_0 = 0, t_1 = \eta, \ldots, t_j = j\eta, \ldots$, and $t_f = L\eta$. According to Eq. (11), the first symplectic approach can be given as follows. Assume that, within the jth subinterval, the state variable $\mathbf{x}(t)$ is approximated by Lagrange polynomials of degree $m-1$ that interpolate m equidistant points, and the costate variable $\boldsymbol{\lambda}(t)$ is approximated by Lagrange polynomials of degree $n-1$ that interpolate n equidistant points; that is,

$$\mathbf{x}\,(t) = (M_1 \otimes \mathbf{I})\mathbf{x}_{j-1} + (\bar{\mathbf{M}} \otimes \mathbf{I})\bar{\mathbf{x}}_j + (M_m \otimes \mathbf{I})\mathbf{x}_j \tag{20}$$

$$\boldsymbol{\lambda}\,(t) = (\mathbf{N} \otimes \mathbf{I})\bar{\boldsymbol{\lambda}}_j \tag{21}$$

in which $\mathbf{I}$ denotes the identity matrix. Vectors $\mathbf{x}_{j-1}$ and $\mathbf{x}_j$ denote the state variables at the left and right ends of the jth subinterval, vector $\bar{\mathbf{x}}_j$ is composed of the state variables at the internal interpolation points within the jth subinterval (i.e., $\bar{\mathbf{x}}_j = \{\bar{\mathbf{x}}_j^2, \bar{\mathbf{x}}_j^3, \cdots, \bar{\mathbf{x}}_j^{m-1}\}^T$), and $\bar{\boldsymbol{\lambda}}_j$ is composed of the costate variables at all of the interpolation points within the jth subinterval (i.e., $\bar{\boldsymbol{\lambda}}_j = \{\bar{\boldsymbol{\lambda}}_j^1, \bar{\boldsymbol{\lambda}}_j^2, \cdots, \bar{\boldsymbol{\lambda}}_j^n\}^T$). Other symbols in Eqs. (20) and (21) are defined as follows:

$$\bar{\mathbf{M}} = [M_2, M_3, \ldots, M_{m-1}] \tag{22}$$

$$\mathbf{N} = [N_1, N_2, \ldots, N_n] \tag{23}$$

$$M_i = \prod_{j=1, j\neq i}^{m} \frac{t - (j-1)\eta/(m-1)}{(i-j)\eta/(m-1)} \tag{24}$$

$$N_i = \prod_{j=1, j\neq i}^{n} \frac{t - (j-1)\eta/(n-1)}{(i-j)\eta/(n-1)} \tag{25}$$

The symbol $\otimes$ in Eqs. (20) and (21) denotes the Kronecker product of two matrices. Substituting the approximate state and costate variables [i.e., Eqs. (20) and (21)] into Eq. (5) gives the following:

$$\bar{S}_j(\mathbf{x}_{j-1}, \mathbf{x}_j, \bar{\mathbf{x}}_j, \bar{\boldsymbol{\lambda}}_j) = \int_0^\eta (\boldsymbol{\lambda}^T \dot{\mathbf{x}} - H(\mathbf{x}, \boldsymbol{\lambda}))_j \mathrm{d}t \qquad j = 1, 2, \cdots, L \tag{26}$$

According to Eq. (11), if the state variables at the two ends of the jth subinterval are taken as the independent variables, and if the Hamiltonian canonical equation is satisfied within the jth subinterval, $\bar{S}$ must be the function of only the state variables at the two ends of the jth subinterval. Hence, for satisfying the Hamiltonian canonical equation, the approximate action $\bar{S}_j(\mathbf{x}_{j-1}, \mathbf{x}_j, \bar{\mathbf{x}}_j, \bar{\boldsymbol{\lambda}}_j)$ in the jth subinterval must be the function of only the state variables at the two ends of the jth subinterval. Therefore, the following equations must be satisfied:

$$\frac{\partial \bar{S}_j(\mathbf{x}_{j-1}, \mathbf{x}_j, \bar{\mathbf{x}}_j, \bar{\boldsymbol{\lambda}}_j)}{\partial \bar{\mathbf{x}}_j} = \mathbf{0}, \qquad j = 1, 2, \cdots, L \tag{27}$$

$$\frac{\partial \bar{S}_j(\mathbf{x}_{j-1}, \mathbf{x}_j, \bar{\mathbf{x}}_j, \bar{\boldsymbol{\lambda}}_j)}{\partial \bar{\boldsymbol{\lambda}}_j} = \mathbf{0}, \qquad j = 1, 2, \cdots, L \tag{28}$$

Moreover, according to Eq. (11), we have

$$\frac{\partial \bar{S}_j(\mathbf{x}_{j-1}, \mathbf{x}_j, \bar{\mathbf{x}}_j, \bar{\boldsymbol{\lambda}}_j)}{\partial \mathbf{x}_{j-1}} + \boldsymbol{\lambda}_{j-1} = \mathbf{0}, \qquad j = 1, 2, \cdots, L \tag{29}$$

$$\frac{\partial \bar{S}_j(\mathbf{x}_{j-1}, \mathbf{x}_j, \bar{\mathbf{x}}_j, \bar{\boldsymbol{\lambda}}_j)}{\partial \mathbf{x}_j} - \boldsymbol{\lambda}_j = \mathbf{0}, \qquad j = 1, 2, \cdots, L \tag{30}$$

So far, based on Eq. (11), the nonlinear TPBVP equation (7) is transformed into a set of nonlinear equations [Eqs. (27–30)]. The nonlinear equations are derived by using the variational principle and the symplectic property; this proof is in the Appendix.

The second symplectic approach can be constructed according to Eq. (15). The state variable $\mathbf{x}(t)$ and the costate variable $\boldsymbol{\lambda}(t)$ within the jth subinterval are approximated by using the Lagrange polynomials with orders $m-1$ and $n-1$, respectively, as follows:

$$\mathbf{x}(t) = (M_1 \otimes \mathbf{I})\mathbf{x}_{j-1} + (\tilde{\mathbf{M}} \otimes \mathbf{I})\bar{\mathbf{x}}_j \tag{31}$$

$$\boldsymbol{\lambda}(t) = (\underset{\sim}{\mathbf{N}} \otimes \mathbf{I})\bar{\boldsymbol{\lambda}}_j + (N_n \otimes \mathbf{I})\boldsymbol{\lambda}_j \tag{32}$$

in which vectors $\mathbf{x}_{j-1}$ and $\boldsymbol{\lambda}_j$ denote the state variable at the left end and the costate variable at the right end of the jth subinterval, vector $\bar{\mathbf{x}}_j$ is defined by $\bar{\mathbf{x}}_j = \{\bar{\mathbf{x}}_j^2, \bar{\mathbf{x}}_j^3, \cdots, \bar{\mathbf{x}}_j^m\}^T$, and $\bar{\boldsymbol{\lambda}}_j$ is defined by $\bar{\boldsymbol{\lambda}}_j = \{\bar{\boldsymbol{\lambda}}_j^1, \bar{\boldsymbol{\lambda}}_j^2, \cdots, \bar{\boldsymbol{\lambda}}_j^{n-1}\}^T$. Other symbols in Eqs. (31) and (32) are defined as follows:

$$\tilde{\mathbf{M}} = [M_2, M_3, \ldots, M_m] \tag{33}$$

$$\underset{\sim}{\mathbf{N}} = [N_1, N_2, \ldots, N_{n-1}] \tag{34}$$

The elements in Eqs. (33) and (34) are the same as those defined in Eqs. (24) and (25). Substituting approximate state variables (31) and costate variables (32) into Eq. (14) gives

$$U_j(\mathbf{x}_{j-1}, \boldsymbol{\lambda}_j, \bar{\mathbf{x}}_j, \bar{\boldsymbol{\lambda}}_j) = \boldsymbol{\lambda}_j^T \bar{\mathbf{x}}_j - \int_0^\eta (\boldsymbol{\lambda}^T \dot{\mathbf{x}} - H(\mathbf{x}, \boldsymbol{\lambda}))_j \mathrm{d}t \qquad j = 1, 2, \cdots, L \tag{35}$$

According to Eq. (15), the approximate action $U_j(\mathbf{x}_{j-1}, \boldsymbol{\lambda}_j, \bar{\mathbf{x}}_j, \bar{\boldsymbol{\lambda}}_j)$ in the jth subinterval must be the function of only the state variable at the left end and the costate variable at the right end of the jth subinterval. Therefore, the following equations must be satisfied:

$$\frac{\partial U_j(\mathbf{x}_{j-1}, \boldsymbol{\lambda}_j, \bar{\mathbf{x}}_j, \bar{\boldsymbol{\lambda}}_j)}{\partial \bar{\mathbf{x}}_j} = \mathbf{0}, \qquad j = 1, 2, \cdots, L \tag{36}$$

$$\frac{\partial U_j(\mathbf{x}_{j-1}, \boldsymbol{\lambda}_j, \bar{\mathbf{x}}_j, \bar{\boldsymbol{\lambda}}_j)}{\partial \bar{\boldsymbol{\lambda}}_j} = \mathbf{0}, \qquad j = 1, 2, \cdots, L \tag{37}$$

In addition, according to Eq. (15), we have

$$\frac{\partial U_j(\mathbf{x}_{j-1}, \boldsymbol{\lambda}_j, \bar{\mathbf{x}}_j, \bar{\boldsymbol{\lambda}}_j)}{\partial \mathbf{x}_{j-1}} - \boldsymbol{\lambda}_{j-1} = \mathbf{0}, \qquad j = 1, 2, \cdots, L \tag{38}$$

$$\frac{\partial U_j(\mathbf{x}_{j-1}, \boldsymbol{\lambda}_j, \bar{\mathbf{x}}_j, \bar{\boldsymbol{\lambda}}_j)}{\partial \boldsymbol{\lambda}_j} - \mathbf{x}_j = \mathbf{0}, \qquad j = 1, 2, \cdots, L \tag{39}$$

Based on Eq. (15), the nonlinear TPBVP equation (7) is transformed into a set of nonlinear equations [Eqs. (36–39)]. It is easy to prove that the approach defined by Eqs. (36–39) is symplectic. The proof is similar to the proof given in the Appendix for the first symplectic approach.

For the third symplectic approach, the approach can be constructed according to Eq. (19). Assume that the state variable $\mathbf{x}(t)$ and the costate variable $\boldsymbol{\lambda}(t)$ within the jth subinterval are approximated by using the Lagrange polynomials with orders $m-1$ and $n-1$, respectively, as follows:

$$\mathbf{x}(t) = (\mathbf{M} \otimes \mathbf{I})\bar{\mathbf{x}}_j \tag{40}$$

$$\boldsymbol{\lambda}(t) = (N_1 \otimes \mathbf{I})\boldsymbol{\lambda}_{j-1} + (\underline{\mathbf{N}} \otimes \mathbf{I})\bar{\boldsymbol{\lambda}}_j + (N_n \otimes \mathbf{I})\boldsymbol{\lambda}_j \tag{41}$$

in which vectors $\boldsymbol{\lambda}_{j-1}$ and $\boldsymbol{\lambda}_j$ denote the costate variables at the left end and the right end of the jth subinterval, vector $\bar{\mathbf{x}}_j$ is defined by $\bar{\mathbf{x}}_j = \{\bar{\mathbf{x}}_j^1, \bar{\mathbf{x}}_j^2, \cdots, \bar{\mathbf{x}}_j^m\}^T$, and $\bar{\boldsymbol{\lambda}}_j$ is defined by $\bar{\boldsymbol{\lambda}}_j = \{\bar{\boldsymbol{\lambda}}_j^2, \bar{\boldsymbol{\lambda}}_j^3, \cdots, \bar{\boldsymbol{\lambda}}_j^{n-1}\}^T$. Other symbols in Eqs. (40) and (41) are defined as follows:

$$\mathbf{M} = [M_1, M_2, \ldots, M_m] \tag{42}$$

$$\underline{\mathbf{N}} = [N_2, N_3, \ldots, N_{n-1}] \tag{43}$$

The elements in Eqs. (42) and (43) are the same as those defined in Eqs. (24) and (25). Substituting approximate state variables (40) and costate variables (41) into Eq. (18) gives the following:

$$V_j(\boldsymbol{\lambda}_{j-1}, \boldsymbol{\lambda}_j, \bar{\mathbf{x}}_j, \bar{\boldsymbol{\lambda}}_j) = \boldsymbol{\lambda}_{j-1}^T \bar{\mathbf{x}}_j^1 - \boldsymbol{\lambda}_j^T \bar{\mathbf{x}}_j^m + \int_0^\eta (\boldsymbol{\lambda}^T \dot{\mathbf{x}} - H(\mathbf{x}, \boldsymbol{\lambda}))_j \mathrm{d}t, \qquad j = 1, 2, \cdots, L \tag{44}$$

According to Eq. (19), the approximate action $V_j(\boldsymbol{\lambda}_{j-1}, \boldsymbol{\lambda}_j, \bar{\mathbf{x}}_j, \bar{\boldsymbol{\lambda}}_j)$ in the jth subinterval must be the function of only the costate variables at the two ends of the jth subinterval. Therefore, the following equations must be satisfied:

$$\frac{\partial V_j(\boldsymbol{\lambda}_{j-1}, \boldsymbol{\lambda}_j, \bar{\mathbf{x}}_j, \bar{\boldsymbol{\lambda}}_j)}{\partial \bar{\mathbf{x}}_j} = \mathbf{0}, \qquad j = 1, 2, \cdots, L \tag{45}$$

$$\frac{\partial V_j(\boldsymbol{\lambda}_{j-1}, \boldsymbol{\lambda}_j, \bar{\mathbf{x}}_j, \bar{\boldsymbol{\lambda}}_j)}{\partial \bar{\boldsymbol{\lambda}}_j} = \mathbf{0}, \qquad j = 1, 2, \cdots, L \tag{46}$$

Then, according to Eq. (19), we have

$$\frac{\partial V_j(\boldsymbol{\lambda}_{j-1}, \boldsymbol{\lambda}_j, \bar{\mathbf{x}}_j, \bar{\boldsymbol{\lambda}}_j)}{\partial \boldsymbol{\lambda}_j} + \mathbf{x}_j = \mathbf{0}, \qquad j = 1, 2, \cdots, L \tag{47}$$

$$\frac{\partial V_j(\boldsymbol{\lambda}_{j-1}, \boldsymbol{\lambda}_j, \bar{\mathbf{x}}_j, \bar{\boldsymbol{\lambda}}_j)}{\partial \boldsymbol{\lambda}_{j-1}} - \mathbf{x}_{j-1} = \mathbf{0}, \qquad j = 1, 2, \cdots, L \tag{48}$$

Based on Eq. (19), the nonlinear TPBVP equation (7) is transformed into a set of nonlinear equations [Eqs. (45–48)], which can also be proved to be symplectic.

IV. Application: Optimal Rendezvous Problem

Consider a spacecraft subject to a central gravity field. To establish the motion equations, we introduce a coordinate frame that is rotating along a circular orbit at a constant angular velocity. The nondimensional dynamical equation can be given by [3]

$$\ddot{x} - 2\dot{y} + (1 + x)\left(\frac{1}{r^3} - 1\right) = u_x \tag{49}$$

$$\ddot{y} + 2\dot{x} + y\left(\frac{1}{r^3} - 1\right) = u_y \tag{50}$$

$$\ddot{z} + \frac{1}{r^3} z = u_z \tag{51}$$

where $r = \sqrt{(x+1)^2 + y^2 + z^2}$. Symbols x, y, and z are the position variables of the spacecraft, and they represent radial, tangential, and normal displacements from the origin of the rotating frame, respectively, and u_x, u_y, and u_z are the control accelerations in the x, y, and z directions of the spacecraft, respectively.

With the nondimensional equations of motion, the goal of the nonlinear optimal control is to minimize the following quadratic cost function; that is,

$$J = \frac{1}{2}\int_0^1 (u_x^2 + u_y^2 + u_z^2)\, \mathrm{d}t \tag{52}$$

In the state space, the state vector is defined as $\mathbf{x} = \{x, y, z, \dot{x}, \dot{y}, \dot{z}\}^T$, and the goal is to transfer the spacecraft from an initial state $\mathbf{x}(0) = \{0.2, 0.2, 0.2, 0.1, 0.1, 0.1\}^T$ to a final state $\mathbf{x}(1) = \{0, 0, 0, 0, 0, 0\}^T$ in a fixed flying time $t_f = 1$ while minimizing the cost function in Eq. (52).

A number of numerical tests shows that the combinations of $m = n + 1$, $m = n$, and $m = n - 1$ for the first, second, and third symplectic approaches are optimal. Therefore, the problem given above is solved by using the three symplectic approaches with $m = 2$, $n = 1$; $m = n = 2$; and $m = 1$, $n = 2$, respectively. Moreover, two different discretion schemes are used; that is, the whole time domain is divided into 8 or 64 time intervals. Figures 1–3 show the state, the costate, and the control history, respectively.

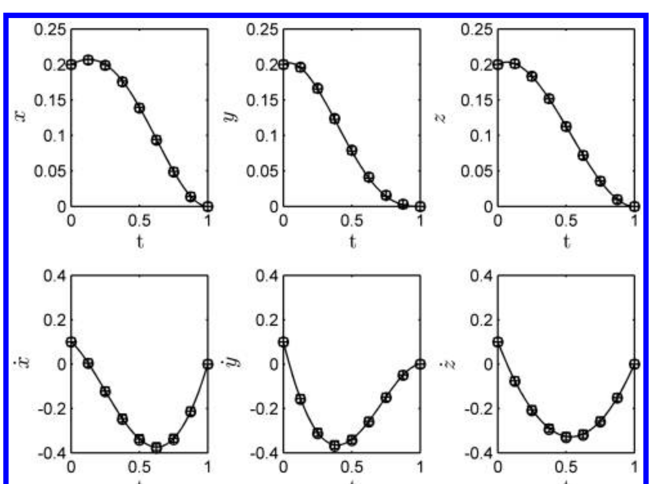

Fig. 1 State trajectory in normalized time.

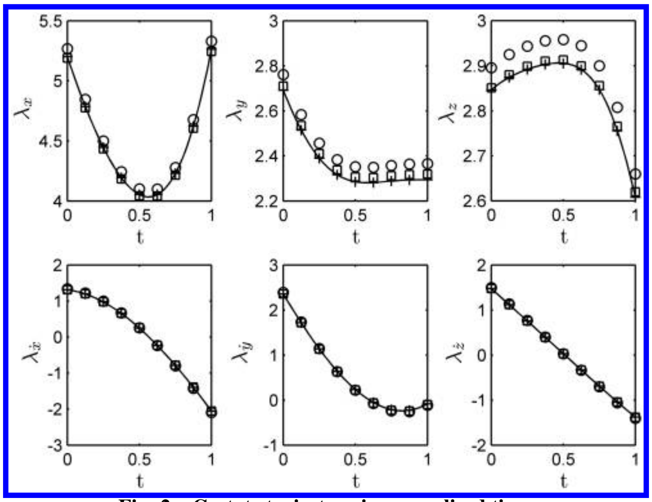

Fig. 2 Costate trajectory in normalized time.

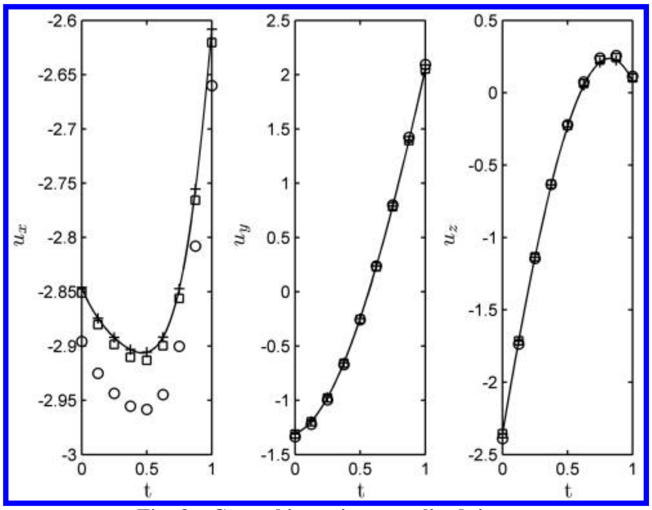

Fig. 3 Control input in normalized time.

When the number of the time intervals is eight, the results from the three different symplectic approaches are given by a circle, a plus, and a square in Figs. 1–3, while when the number of the time intervals is 64, the results from the three different symplectic approaches are given by the solid, dashed, and dotted lines in Figs. 1–3. Figures 1–3 show that the three symplectic approaches give different numerical results when the number of the time intervals is small, while all three approaches give almost the same results (mixed with each other) when the number of the time intervals is larger. Moreover, Fig. 1 shows that both the initial and terminal conditions are satisfied very well.

Table 1 Cost functions for different time intervals

Number of intervals	First symplectic approach	Second symplectic approach	Third symplectic approach
8	10.399283	10.037657	10.081721
16	10.158212	10.069116	10.080302
32	10.099259	10.077067	10.079874
64	10.084601	10.079058	10.079760
128	10.080941	10.079556	10.079731
256	10.080027	10.079680	10.079724
512	10.079798	10.079712	10.079722
1024	10.079741	10.079719	10.079722
2048	10.079727	10.079721	10.079722
4096	10.079723	10.079722	10.079722
8192	10.079722	10.079722	10.079722

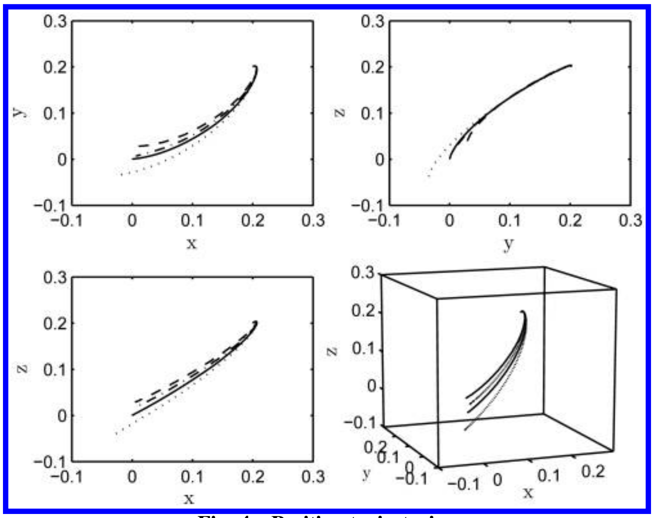

Fig. 4 Position trajectories.

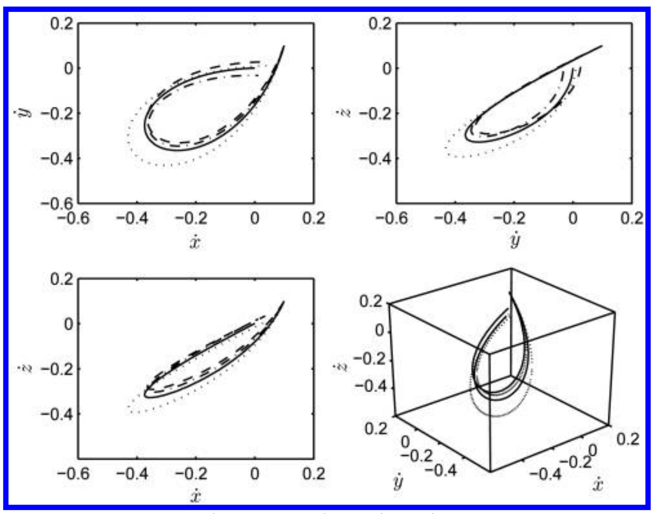

Fig. 5 Velocity trajectories.

To see more differences of the above three symplectic approaches, Table 1 shows the cost function changing with changes in the number of time intervals. When the number of time intervals is increased, all three symplectic approaches tend to convergence and converge to the same value.

For this example, some numerical comparisons between the proposed symplectic methods and the generating function method [3] are given in Figs. 4 and 5. The solid lines are the results given by the first symplectic method with 64 time intervals, and the dashed, dotted, and dashed–dotted lines are the results given by the first-, second-, and third-order generating function methods, respectively. Figures 4 and 5 show that the terminal values of positions and trajectories obtained by the proposed method satisfy the terminal boundary conditions. For the generating function method, terminal values of positions and trajectories with the increasing of the number of Taylor series expansions terms tend to satisfy the terminal boundary conditions. Although, terminal boundary conditions cannot be satisfied accurately by the generating function method, the generating function method can give a feedback control law, and so it is a closed-loop method.

V. Conclusions

Three different symplectic numerical approaches are proposed based on the variational principle to solve TPBVP in optimal control. The three symplectic approaches are constructed by choosing different types of independent variables at the two ends of a time step. For each approach, the nonlinear TPBVP is transformed into a set of nonlinear algebraic equations that can preserve the symplectic structure of the original Hamiltonian system. The proposed symplectic approaches are successfully applied to solve optimal orbital rendezvous problems in a central gravity field. The numerical results show that the three symplectic approaches give different numerical performances; however, with an increase in the number of time intervals, all three symplectic approaches give the same convergence results.

Appendix: Symplectic Property of the First Approach

It is easy to verify that Eq. (10) is equivalent to the following three equations:

$$\left(\frac{\partial \mathbf{x}_j}{\partial \mathbf{x}_{j-1}}\right)^T \frac{\partial \boldsymbol{\lambda}_j}{\partial \mathbf{x}_{j-1}} = \left[\left(\frac{\partial \mathbf{x}_j}{\partial \mathbf{x}_{j-1}}\right)^T \frac{\partial \boldsymbol{\lambda}_j}{\partial \mathbf{x}_{j-1}}\right]^T \tag{A1}$$

$$\left(\frac{\partial \mathbf{x}_j}{\partial \boldsymbol{\lambda}_{j-1}}\right)^T \frac{\partial \boldsymbol{\lambda}_j}{\partial \boldsymbol{\lambda}_{j-1}} = \left[\left(\frac{\partial \mathbf{x}_j}{\partial \boldsymbol{\lambda}_{j-1}}\right)^T \frac{\partial \boldsymbol{\lambda}_j}{\partial \boldsymbol{\lambda}_{j-1}}\right]^T \tag{A2}$$

$$\left(\frac{\partial \mathbf{x}_j}{\partial \mathbf{x}_{j-1}}\right)^T \frac{\partial \boldsymbol{\lambda}_j}{\partial \boldsymbol{\lambda}_{j-1}} - \left(\frac{\partial \boldsymbol{\lambda}_j}{\partial \mathbf{x}_{j-1}}\right)^T \frac{\partial \mathbf{x}_j}{\partial \boldsymbol{\lambda}_{j-1}} = \mathbf{I} \tag{A3}$$

Next, we will prove that the numerical approach defined by Eqs. (27–30) satisfies Eqs. (A1–A3).

Step 1: Within an arbitrary interval j, assume that the variables $\bar{\mathbf{x}}_j$, $\bar{\boldsymbol{\lambda}}_j$, $\mathbf{x}_j$, and $\boldsymbol{\lambda}_j$ are all functions of the variables $\mathbf{x}_{j-1}$ and $\boldsymbol{\lambda}_{j-1}$. Then, based on the chain rule of derivatives, taking a derivative of Eqs. (27–30) with respect to variable $\mathbf{x}_{j-1}$ gives the following:

$$\boldsymbol{\Omega}_1 \mathbf{X} + \boldsymbol{\Omega}_2^T = \left\{ \mathbf{0} \quad \mathbf{0} \quad \left(\frac{\partial \boldsymbol{\lambda}_j}{\partial \mathbf{x}_{j-1}}\right)^T \right\}^T \tag{A4}$$

$$\boldsymbol{\Omega}_2 \mathbf{X} = -\frac{\partial^2 \bar{S}_j}{\partial \mathbf{x}_{j-1} \partial \mathbf{x}_{j-1}} \tag{A5}$$

in which

$$\boldsymbol{\Omega}_1 = \begin{bmatrix} \frac{\partial^2 \bar{S}_j}{\partial \bar{\mathbf{x}}_j \partial \bar{\mathbf{x}}_j} & \frac{\partial^2 \bar{S}_j}{\partial \bar{\mathbf{x}}_j \partial \bar{\boldsymbol{\lambda}}_j} & \frac{\partial^2 \bar{S}_j}{\partial \bar{\mathbf{x}}_j \partial \mathbf{x}_j} \\ \frac{\partial^2 \bar{S}_j}{\partial \bar{\boldsymbol{\lambda}}_j \partial \bar{\mathbf{x}}_j} & \frac{\partial^2 \bar{S}_j}{\partial \bar{\boldsymbol{\lambda}}_j \partial \bar{\boldsymbol{\lambda}}_j} & \frac{\partial^2 \bar{S}_j}{\partial \bar{\boldsymbol{\lambda}}_j \partial \mathbf{x}_j} \\ \frac{\partial^2 \bar{S}_j}{\partial \mathbf{x}_j \partial \bar{\mathbf{x}}_j} & \frac{\partial^2 \bar{S}_j}{\partial \mathbf{x}_j \partial \bar{\boldsymbol{\lambda}}_j} & \frac{\partial^2 \bar{S}_j}{\partial \mathbf{x}_j \partial \mathbf{x}_j} \end{bmatrix} \tag{A6}$$

$$\boldsymbol{\Omega}_2 = \left\{ \frac{\partial^2 \bar{S}_j}{\partial \mathbf{x}_{j-1} \partial \bar{\mathbf{x}}_j} \quad \frac{\partial^2 \bar{S}_j}{\partial \mathbf{x}_{j-1} \partial \bar{\boldsymbol{\lambda}}_j} \quad \frac{\partial^2 \bar{S}_j}{\partial \mathbf{x}_{j-1} \partial \mathbf{x}_j} \right\} \tag{A7}$$

$$\mathbf{X} = \left\{ \left(\frac{\partial \bar{\mathbf{x}}_j}{\partial \mathbf{x}_{j-1}}\right)^T \quad \left(\frac{\partial \bar{\boldsymbol{\lambda}}_j}{\partial \mathbf{x}_{j-1}}\right)^T \quad \left(\frac{\partial \mathbf{x}_j}{\partial \mathbf{x}_{j-1}}\right)^T \right\}^T \tag{A8}$$

Similarly, taking the derivative of Eqs. (27–30) with respect to variable $\boldsymbol{\lambda}_{j-1}$ gives

$$\boldsymbol{\Omega}_1 \mathbf{Y} = \left\{ \mathbf{0} \quad \mathbf{0} \quad \left(\frac{\partial \boldsymbol{\lambda}_j}{\partial \boldsymbol{\lambda}_{j-1}}\right)^T \right\}^T \tag{A9}$$

$$\boldsymbol{\Omega}_2 \mathbf{Y} = -\mathbf{I} \tag{A10}$$

$$\mathbf{Y} = \left\{ \left(\frac{\partial \bar{\mathbf{x}}_j}{\partial \boldsymbol{\lambda}_{j-1}}\right)^T \quad \left(\frac{\partial \bar{\boldsymbol{\lambda}}_j}{\partial \boldsymbol{\lambda}_{j-1}}\right)^T \quad \left(\frac{\partial \mathbf{x}_j}{\partial \boldsymbol{\lambda}_{j-1}}\right)^T \right\}^T \tag{A11}$$

Left multiplying on both sides of Eq. (A4) by the transpose of **X** gives

$$\mathbf{X}^T\mathbf{\Omega}_1\mathbf{X} + \mathbf{X}^T\mathbf{\Omega}_2^T = \left(\frac{\partial \mathbf{x}_j}{\partial \mathbf{x}_{j-1}}\right)^T \frac{\partial \boldsymbol{\lambda}_j}{\partial \mathbf{x}_{j-1}} \tag{A12}$$

Substituting Eq. (A5) into Eq. (A12) gives

$$\mathbf{X}^T\mathbf{\Omega}_1\mathbf{X} - \frac{\partial^2 \bar{S}_j}{\partial \mathbf{x}_{j-1}\partial \mathbf{x}_{j-1}} = \left(\frac{\partial \mathbf{x}_j}{\partial \mathbf{x}_{j-1}}\right)^T \frac{\partial \boldsymbol{\lambda}_j}{\partial \mathbf{x}_{j-1}} \tag{A13}$$

The matrices $\mathbf{\Omega}_1$ and $\partial^2 \bar{S}_j/\partial \mathbf{x}_{j-1}\partial \mathbf{x}_{j-1}$ are both symmetric matrices, so the matrix $(\partial \boldsymbol{\lambda}_j/\partial \mathbf{x}_{j-1})^T(\partial \mathbf{x}_j/\partial \mathbf{x}_{j-1})$ in Eq. (A13) is also a symmetric matrix, which means that the approach satisfies Eq. (A1).

Step 2: Left multiplying on both sides of Eq. (A9) by the transpose of **Y** gives

$$\mathbf{Y}^T\mathbf{\Omega}_1\mathbf{Y} = \left(\frac{\partial \mathbf{x}_j}{\partial \boldsymbol{\lambda}_{j-1}}\right)^T \frac{\partial \boldsymbol{\lambda}_j}{\partial \boldsymbol{\lambda}_{j-1}} \tag{A14}$$

The matrix $\mathbf{\Omega}_1$ is a symmetric matrix, so the matrix $(\partial \mathbf{x}_j/\partial \boldsymbol{\lambda}_{j-1})^T(\partial \boldsymbol{\lambda}_j/\partial \boldsymbol{\lambda}_{j-1})$ is also a symmetric matrix, which means that the approach satisfies Eq. (A2).

Step 3: Left multiplying on both sides of Eq. (A9) by the transpose of **X** gives

$$\mathbf{X}^T\mathbf{\Omega}_1\mathbf{Y} = \left(\frac{\partial \mathbf{x}_j}{\partial \mathbf{x}_{j-1}}\right)^T \frac{\partial \boldsymbol{\lambda}_j}{\partial \boldsymbol{\lambda}_{j-1}} \tag{A15}$$

Transposing both sides of Eq. (A4) and then multiplying **Y** gives

$$\mathbf{X}^T\mathbf{\Omega}_1\mathbf{Y} + \mathbf{\Omega}_2\mathbf{Y} = \left(\frac{\partial \boldsymbol{\lambda}_j}{\partial \mathbf{x}_{j-1}}\right)^T \frac{\partial \mathbf{x}_j}{\partial \boldsymbol{\lambda}_{j-1}} \tag{A16}$$

Substituting Eq. (A10) into Eq. (A16) and then subtracting Eq. (A16) from Eq. (A15) gives

$$\left(\frac{\partial \mathbf{x}_j}{\partial \mathbf{x}_{j-1}}\right)^T \frac{\partial \boldsymbol{\lambda}_j}{\partial \boldsymbol{\lambda}_{j-1}} - \left(\frac{\partial \boldsymbol{\lambda}_j}{\partial \mathbf{x}_{j-1}}\right)^T \frac{\partial \mathbf{x}_j}{\partial \boldsymbol{\lambda}_{j-1}} = \mathbf{I} \tag{A17}$$

Equation (A17) shows that the approach satisfies Eq. (A3).

We proved that the numerical approach defined by Eqs. (27–30) satisfies Eqs. (A1–A3), so it is a symplectic approach.

Acknowledgments

The authors are grateful for the financial support of the National Science Foundation of China (11102031, 10902020, and 11072044), the National Basic Research Program of China (973 Program 2010CB832704), and the Fundamental Research Funds for the Central Universities (DUT11ZD(G)02).

References

[1] Guibout, V. M., and Scheeres, D. J., "Solving Relative Two-Point Boundary Value Problems Spacecraft Formation Flight Transfers Application," *Journal of Guidance, Control, and Dynamics*, Vol. 27, No. 4, 2004, pp. 693–704.
doi:10.2514/1.11164

[2] Huntington, G. T., and Rao, A. V., "Optimal Reconfiguration of Spacecraft Formations Using the Gauss Pseudospectral Method," *Journal of Guidance, Control, and Dynamics*, Vol. 31, No. 3, 2008, pp. 689–698.
doi:10.2514/1.31083

[3] Park, C., Guibout, V., and Scheeres, D. J., "Solving Optimal Continuous Thrust Rendezvous Problems with Generating Functions," *Journal of Guidance, Control, and Dynamics*, Vol. 29, No. 2, 2006, pp. 321–331.
doi:10.2514/1.14580

[4] Betts, J. T., "Survey of Numerical Methods for Trajectory Optimization," *Journal of Guidance, Control, and Dynamics*, Vol. 21, No. 2, 1998, pp. 193–207.
doi:10.2514/2.4231

[5] Hodges, D. H., and Bless, R. R., "Weak Hamiltonian Finite Element Method for Optimal Control Problems," *Journal of Guidance, Control, and Dynamics*, Vol. 14, No. 1, 1991, pp. 148–156.
doi:10.2514/3.20616

[6] Armellin, R., and Topputo, F., "A Sixth-Order Accurate Scheme for Solving Two-Point Boundary Value Problems in Astrodynamics," *Celestial Mechanics and Dynamical Astronomy*, Vol. 96, 2006, pp. 289–309.
doi:10.1007/s10569-006-9047-4

[7] Majji, M., Turner, J. D., and Junkins, J. L., "Solution of Two-Point Boundary-Value Problems using Lagrange Implicit Function Theorem," *Journal of Guidance, Control, and Dynamics*, Vol. 32, No. 5, 2009, pp. 1684–1687.
doi:10.2514/1.43024

[8] Bryson, A. E., and Ho, Y. C., *Applied Optimal Control: Optimization, Estimation and Control*, Hemisphere, Washington, D. C., 1975, pp. 42–87.

[9] Arnold, V. I., *Mathematical Methods of Classical Mechanics*, Springer–Verlag, New York, 1989, pp. 233–266.

[10] Hairer, E., Lubich, C., and Wanner, G., *Geometric Numerical Integration: Structure-Preserving Algorithm for Ordinary Differential Equations*, Springer, New York, 2006, pp. 179–227.

[11] Ober-Blöbaum, S., Junge, O., and Marsden, J. E., "Discrete Mechanics and Optimal Control: An Analysis," *ESAIM: Control, Optimisation and Calculus of Variations*, Vol. 17, No. 2, 2011, pp. 322–352.
doi:10.1051/cocv/2010012

[12] Moore, A., Ober-Blöbaum, S., and Marsden, J. E., "Mesh Refinement Strategies for Spacecraft Trajectory Optimization Using Discrete Mechanics and Optimal Control," *21st AAS/AIAA Space Flight Mechanics Meeting*, New Orleans, LA, American Astronomical Soc., Washington, D.C., 2011, pp. 361–380.

This article has been cited by:

1. Boyang Shi, Haijun Peng, Xinwei Wang, Wanxie Zhong. 2022. A symplectic direct method for motion-driven optimal control of mechanical systems. *Communications in Nonlinear Science and Numerical Simulation* **111**, 106501. [Crossref]
2. Xinwei Wang, Jie Liu, Xianzhou Dong, Chongwei Li, Yong Zhang. 2021. A symplectic pseudospectral method for constrained time-delayed optimal control problems and its application to biological control problems. *Optimization* **70**:12, 2527-2557. [Crossref]
3. Paul Kotyczka, Tobias Thoma. 2021. Symplectic discrete-time energy-based control for nonlinear mechanical systems. *Automatica* **133**, 109842. [Crossref]
4. Da Jiang, Zhiqin Cai, Haijun Peng, Zhigang Wu. 2021. Coordinated Control Based on Reinforcement Learning for Dual-Arm Continuum Manipulators in Space Capture Missions. *Journal of Aerospace Engineering* **34**:6. . [Crossref]
5. Xinwei Wang, Jie Liu, Haijun Peng, Lingchong Gao, Johannes Fottner, Pengliang Liu. 2021. Input-constrained chaos synchronization of horizontal platform systems via a model predictive controller. *Proceedings of the Institution of Mechanical Engineers, Part C: Journal of Mechanical Engineering Science* **235**:20, 4862-4872. [Crossref]
6. M. A. Mehrpouya, R. Salehi. 2021. A numerical scheme based on the collocation and optimization methods for accurate solution of sensitive boundary value problems. *The European Physical Journal Plus* **136**:9. . [Crossref]
7. Mohammad Ali Mehrpouya, Haijun Peng. 2021. A robust pseudospectral method for numerical solution of nonlinear optimal control problems. *International Journal of Computer Mathematics* **98**:6, 1146-1165. [Crossref]
8. Boyang Shi, Haijun Peng, Xinwei Wang, Wanxie Zhong, Lingchong Gao, Johannes Fottner. 2021. A symplectic indirect approach for a class of nonlinear optimal control problems of differential-algebraic systems. *International Journal of Robust and Nonlinear Control* **31**:7, 2712-2736. [Crossref]
9. M. Shahini, M.A. Mehrpouya. 2021. Transformed orthogonal functions for solving infinite horizon fractional optimal control problems. *European Journal of Control* **59**, 13-28. [Crossref]
10. Donghun Lee, Young-Joo Song. 2021. Influence of Steering Angle Profiles on the Orbit Transfer Trajectory. *Mathematical Problems in Engineering* **2021**, 1-12. [Crossref]
11. Xinwei Wang, Jie Liu, Haijun Peng. SPM for Unconstrained Nonlinear Optimal Control Problems 33-51. [Crossref]
12. Long Cheng, Hao Wen, Dongping Jin. 2020. Reconfiguration control of satellite formation using online quasi-linearization iteration and symplectic discretization. *Aerospace Science and Technology* **107**, 106348. [Crossref]
13. Zhong Wang, Yan Li. 2020. Rigid spacecraft robust optimal attitude stabilization under actuator misalignments. *Aerospace Science and Technology* **105**, 105990. [Crossref]
14. Zhong Wang, Yan Li. 2020. Rigid spacecraft robust adaptive attitude Stabilization Using state-dependent indirect Chebyshev pseudospectral method. *Acta Astronautica* **174**, 94-102. [Crossref]
15. Zhong Wang, Yan Li. 2020. Guaranteed cost spacecraft attitude stabilization under actuator misalignments using linear partial differential equations. *Journal of the Franklin Institute* **357**:10, 6018-6040. [Crossref]
16. Mohammad A Mehrpouya. 2020. A modified pseudospectral method for indirect solving a class of switching optimal control problems. *Proceedings of the Institution of Mechanical Engineers, Part G: Journal of Aerospace Engineering* **234**:9, 1531-1542. [Crossref]
17. Jie Liu, Wei Han, Xinwei Wang, Jie Li. 2020. Research on Cooperative Trajectory Planning and Tracking Problem for Multiple Carrier Aircraft on the Deck. *IEEE Systems Journal* **14**:2, 3027-3038. [Crossref]
18. Haijun Peng, Fei Li, Jinguo Liu, Zhaojie Ju. 2020. A Symplectic Instantaneous Optimal Control for Robot Trajectory Tracking With Differential-Algebraic Equation Models. *IEEE Transactions on Industrial Electronics* **67**:5, 3819-3829. [Crossref]
19. Minqiang Xu, Jing Niu, Li Guo. 2020. A High-Order Numerical Method for a Nonlinear System of Second-Order Boundary Value Problems. *Mathematical Problems in Engineering* **2020**, 1-7. [Crossref]
20. ZhiBo E, Davide Guzzetti. 2020. Multi-revolution low-thrust trajectory optimization using symplectic methods. *Science China Technological Sciences* **63**:3, 506-519. [Crossref]
21. Sheng Zhang, En-Mi Yong, Wei-Qi Qian, Kai-Feng He. 2019. A Variation Evolving Method for Optimal Control Computation. *Journal of Optimization Theory and Applications* **183**:1, 246-270. [Crossref]
22. Haijun Peng, Boyang Shi, Xinwei Wang, Chao Li. 2019. Interval estimation and optimization for motion trajectory of overhead crane under uncertainty. *Nonlinear Dynamics* **96**:2, 1693-1715. [Crossref]

23. Jie Liu, Wei Han, Haijun Peng, Xinwei Wang. 2019. Trajectory planning and tracking control for towed carrier aircraft system. *Aerospace Science and Technology* **84**, 830-838. [Crossref]
24. Jianjun Sui, Junbo Chen, Xiaoxiao Zhang, Guohua Nie, Teng Zhang. 2019. Symplectic Analysis of Wrinkles in Elastic Layers With Graded Stiffnesses. *Journal of Applied Mechanics* **86**:1. . [Crossref]
25. Yan Li, Zhong Wang. An Adaptive Cross Approximation-based Method for Robust Nonlinear Feedback Control Problems 3460-3465. [Crossref]
26. Jie Liu, Wei Han, Chun Liu, Haijun Peng. 2018. A New Method for the Optimal Control Problem of Path Planning for Unmanned Ground Systems. *IEEE Access* **6**, 33251-33260. [Crossref]
27. Jie Liu, Wei Han, Yong Zhang, Zhigang Chen, Haijun Peng. 2018. Design of an Online Nonlinear Optimal Tracking Control Method for Unmanned Ground Systems. *IEEE Access* **6**, 65429-65438. [Crossref]
28. Haijun Peng, Chao Li. 2017. Bound Evaluation for Spacecraft Swarm on Libration Orbits with an Uncertain Boundary. *Journal of Guidance, Control, and Dynamics* **40**:10, 2690-2698. [Citation] [Full Text] [PDF] [PDF Plus]
29. Haijun Peng, Xinwei Wang, Sheng Zhang, Biaosong Chen. 2017. An iterative symplectic pseudospectral method to solve nonlinear state-delayed optimal control problems. *Communications in Nonlinear Science and Numerical Simulation* **48**, 95-114. [Crossref]
30. Zhong Wang, Yan Li. 2017. An Indirect Method for Inequality Constrained Optimal Control Problems * *This work is supported by the National Natural Science Foundation of China (No. 61473233). *IFAC-PapersOnLine* **50**:1, 4070-4075. [Crossref]
31. Haijun Peng, Xinwei Wang, Mingwu Li, Biaosong Chen. 2017. An hp symplectic pseudospectral method for nonlinear optimal control. *Communications in Nonlinear Science and Numerical Simulation* **42**, 623-644. [Crossref]
32. Abolfazl Shirazi. 2016. Trajectory optimization of spacecraft high-thrust orbit transfer using a modified evolutionary algorithm. *Engineering Optimization* **48**:10, 1639-1657. [Crossref]
33. Lei Zhang, Bo Xu, Muzi Li, Fei Zhang. 2016. Semi-analytical approach for computing near-optimal low-thrust transfers to geosynchronous orbit. *Aerospace Science and Technology* **55**, 482-493. [Crossref]
34. Mingwu Li, Haijun Peng. 2016. Solutions of nonlinear constrained optimal control problems using quasilinearization and variational pseudospectral methods. *ISA Transactions* **62**, 177-192. [Crossref]
35. Mingwu Li, Haijun Peng, Wanxie Zhong. 2016. Optimal control of loose spacecraft formations near libration points with collision avoidance. *Nonlinear Dynamics* **83**:4, 2241-2261. [Crossref]
36. Haijun Peng, Xin Jiang. 2016. Nonlinear receding horizon guidance for spacecraft formation reconfiguration on libration point orbits using a symplectic numerical method. *ISA Transactions* **60**, 38-52. [Crossref]
37. Mingwu Li, Haijun Peng, Zhigang Wu. 2015. Symplectic Irregular Interpolation Algorithms for Optimal Control Problems. *International Journal of Computational Methods* **12**:06, 1550040. [Crossref]
38. Haijun Peng, Qiang Gao, Zhigang Wu, Wanxie Zhong. 2015. Symplectic algorithms with mesh refinement for a hypersensitive optimal control problem. *International Journal of Computer Mathematics* **92**:11, 2273-2289. [Crossref]
39. Jing Li, Xiao-ning Xi. 2015. Time-optimal reorientation of the rigid spacecraft using a pseudospectral method integrated homotopic approach. *Optimal Control Applications and Methods* **36**:6, 889-918. [Crossref]
40. Mingwu Li, Haijun Peng, Wanxie Zhong. 2015. A symplectic sequence iteration approach for nonlinear optimal control problems with state-control constraints. *Journal of the Franklin Institute* **352**:6, 2381-2406. [Crossref]
41. Rui Li, Xiaoqin Ni, Gengdong Cheng. 2015. Symplectic Superposition Method for Benchmark Flexure Solutions for Rectangular Thick Plates. *Journal of Engineering Mechanics* **141**:2. . [Crossref]
42. Xin Du, Hai-Yang Li, Yue-Chen Huang. 2015. Efficient Nonlinear Algorithm for Drag Tracking in Entry Guidance. *Procedia Engineering* **99**, 1014-1026. [Crossref]
43. I. Shafieenejad, A.B. Novinzadeh, V.R. Molazadeh. 2014. Comparing and analyzing min-time and min-effort criteria for free true anomaly of low-thrust orbital maneuvers with new optimal control algorithm. *Aerospace Science and Technology* **35**, 116-134. [Crossref]
44. Haijun Peng, Xin Jiang, Biaosong Chen. 2014. Optimal nonlinear feedback control of spacecraft rendezvous with finite low thrust between libration orbits. *Nonlinear Dynamics* **76**:2, 1611-1632. [Crossref]
45. Haijun Peng, Qiang Gao, Zhigang Wu, Wanxie Zhong. 2013. Efficient Sparse Approach for Solving Receding-Horizon Control Problems. *Journal of Guidance, Control, and Dynamics* **36**:6, 1864-1872. [Citation] [Full Text] [PDF] [PDF Plus]